XMM Flight Mirror Modules environmental and optical testing

Y. Stockman, I. Domken, H. Hansen, J. Ph. Tock
CSL, Centre Spatial de Liege – University of Liege
B- 4031 Angleur (Liege)
Belgium
phone : 32 4 3676668, fax : 32 4 3675613, email : ystockman@ulg.ac.be.

D. de Chambure, Ph. Gondoin
ESA / ESTEC / XMM Project
PO BOX 299, 2200 AG Noordwijk, ZH
The Netherlands

ABSTRACT

The X-ray Multi-Mirror Mission is one of the four "Cornerstone" projects in the ESA Long-Term Program for Space Science. Presently, five XMM Mirror Modules (MM) (including one Qualification Model) have been tested in the FOCALX facility of CSL. The MMs are illuminated by a vertical EUV (58.4 nm) collimated beam allowing to get the optical performance in an effective flight configuration. To fully analyse the MM characteristics, reflectivity measurements are performed in X-ray thanks to a pencil beam. The reflectivity measurements of single shell are performed at Al, Au, Cu, Mo lines between 1.5 and 13 keV. This information is used to evaluate the effective area in X-rays. Wing scattering measurements are performed and show a good correlation with the Power Spectral Density measured with a PROMAP microscope interferometer during mirror shell manufacturing.
This paper deals first with the presentation and comparison of the results achieved on the five MMs. In a second step the results of complementary tests, performed to cross check the data and to get a better understanding of the MM behaviour, are discussed.

KEYWORDS :
X-ray optics and telescope, EUV optics, test facility, XMM

1. INTRODUCTION

The X-ray Multi Mirror Mission[1,2,3] (XMM) has been designed to be a high throughput spectroscopy mission over a broad energy band ranging from 0.1 to 12 keV. The payload includes three co-aligned grazing incidence telescopes made of 58 nested Wolter I mirror shells (MS) achieving an effective collecting area higher than 4200 cm_ at 2 keV and 1800 cm_ at 8 keV. The requirements of a Mirror Module (MM) are presented in Table 1. Two of the three telescopes will be equipped with a grating assembly for spectroscopy measurement. Sources outside the field of view give straylight in the focal plane by single reflection from one or more of the hyperbola mirror. In order to decrease the straylight, a set of 'sieve plates', called X-Ray Baffle (XRB), made out of circular strips[4] is located in front of each MM.
Up to now, five MMs have been built, one Qualification Model (QM) including only 21 active optical MSs and 37 dummy MSs, and 4 Flight Models (FM). The required specifications have to be fulfilled in orbit, but have to be demonstrated on ground. To verify the performance of every MM a set of tests have been planned and performed at CSL on each MM.
The main tests are optical measurements to entirely characterise the MMs. A vertical EUV collimated beam that fully illuminates the mirror module is used. To measure local reflectivity at several energies an X-ray pencil beam is used. The environmental impact on the FM MMs is evaluated by simulating the launch vibration, and the thermal environment in orbit. After these environmental tests a new standard optical test and complementary optical tests are performed to fully characterise the MMs with the XRB before launch.

These latter tests allow to select the 3 best FM MMs out of the 4, to be integrated on the satellite, but also to certify and improve the numerical model of XMM[11]. In 1995-96, a QM of an XMM MM was manufactured and has been characterised at CSL during 96. In 97, the optical performance of 3 FM MMs have been fully verified in the same facility. In addition, the characterisation of FM1 MM equipped with the FM1 reflection grating assembly box (RGA) has been carried out. During January 98, complementary experiments on FM1 MM + XRB were accomplished. The integration of XRB on FM2 MM has been realised and controlled, a test of FM2 MM + FM2 XRB + FM2 RGA in flight configuration, with environmental simulation has been conducted. Finally the FM4 MM has been characterised. The full set of acceptance tests on FM3 and FM4 MMs added with the XRB and the respected RGA FM, are planned to be finished before the end of 1998.

Table 1 : MM Requirements

Focal length	7500 mm
Resolution	
Half Energy Width	16 arcsec (0.1 - 12 keV)
Full Width Half Max	8 arcsec (0.1 - 12 keV)
Effective area	1475 cm_ at 1.5 keV
	580 cm_ at 8 keV
Reflective coating	Gold (250 nm)
Mirror diameter	
outermost	700 mm
innermost	306 mm
Axial parabola length	300 mm
Axial hyperbola length	300 mm
Mirror thickness	0.47 – 1.07 mm
Packing distance	1 – 5 mm
Numbers of mirrors	58
Mirror Module Mass	425 kg

This paper describes the characterisation of the 5 MMs and compares their performance. As already reported[8], the environmental tests have no impact on the MMs optical quality. The tests with the RGA are presented in ref. 5. The test configuration[6,7] is shortly summarised. The second part of this paper presents complementary tests, allowing a deeper characterisation of the MMs equipped with XRB.

2. ENVIRONMENTAL TESTS ON THE MIRROR MODULES

The test sequence on each MM is the following. A first systematic optical reference test is performed. This provides preliminary optical characterisation of the MM. This set of information is used as reference to check the impact of the environmental tests. Afterwards, the environmental tests are performed which consist in three (6 for the QM) thermal cycles between -15°C and + 40°C (about 60 hours per cycle) and a vibration test. For QM and FM1 MMs, an optical reference was performed between the environmental tests. This was not performed for FM2, 3 and 4 since no degradation of the MM performance was observed[8].
For vibration tests, the MMs are submitted to sinusoidal and random vibrations along the X (optical axis), Y and Z at acceptance level for all the FM. The levels are : 10 g along axial X axis and 6.7 g along lateral Y, Z axes. The results are summarised in the Table 2, and the achieved values correspond to those expected from the mathematical model. A last optical reference is then performed.

Table 2 : Vibration test results on MMs

QM / FM1 / FM2 / FM3/ FM4 VIBRATION			
	X axis	Y axis	Z axis
Max sine input [g]	10.1 / 10 / 10 / 10 / 10	10 / 6.7 / 6.8 / 6.8 / 5.7	10 / 6.8 / 6.8 / 6.8 / 6.0
Max sine response [g]	18.6 / 15.1 / 14.9 / 15.1 / 14.8	15.5 / 10.4 / 9 / 9.3 / 10.3	17.2 / 10.6 / 10.6 / 10.5 / 10.5
Location	Spider centre	blocking shell	blocking shell
Max rand. Response [grms]	8.4 / 5.6 /6.8 / 6 / 7.3	5.2 / 4.4 / 4.5 / 3.8 / 4.7	6.3 / 4.7 / 4.2 / 3.1 / 4.1
Location	MSP I/F frame	blocking shell	blocking shell
Fundamental freq. [Hz]	110 / 113 / 112 / 113 / 115	53 / 55 / 54 / 55 / 55	53 / 54 / 54 / 55 /55

3. EUV MEASUREMENTS

3.1. Introduction

A full parallel beam illumination can not be achieved in the X-ray domain. The visible domain is limited by diffraction due to the highly nested MM design. The solution is to use Extreme Ultra Violet (EUV) light. This solution has the advantage to deal with standard hardware. The use of a vertical facility[9, 2] minimises the effect of gravity on the very thin mirrors. This EUV collimator is utilised to measure the Point Spread Function (PSF) at nominal focus, but also to measure the focal length and the PSF at the best focus and in the Field Of View (FOV). The homogeneity transmission of the MM, the effective area on axis and off axis, the orientation of the alignment lens with respect to the maximum throughput are also calibrated. The design of the facility was made to allow the measurement of the straylight and the efficiency of the XRB. The results and analysis of all these tests will be presented hereafter.

3.2. Set-up description

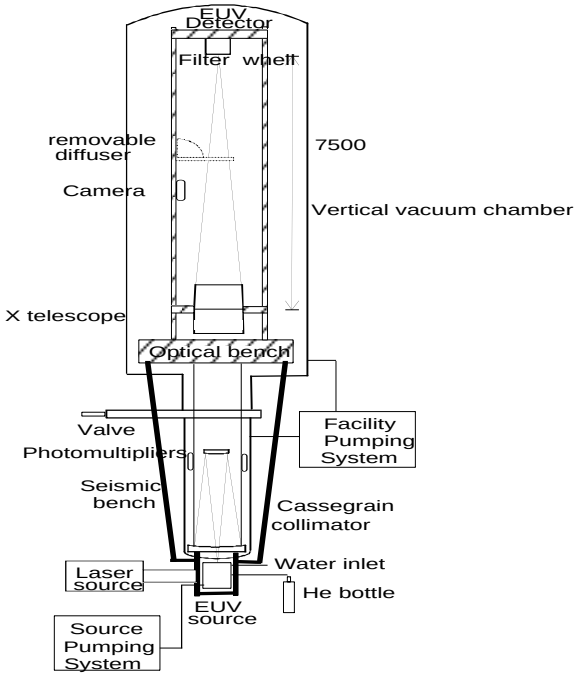

Figure 1 : EUV channel general layout

The set-up is largely described in 6,7, and consists mainly in an Electron Cyclotron Resonance source providing He lines at 58.4 and 30.4 nm, that illuminates a Cassegrain collimator through a 100 µm diameter pinhole. This collimated beam is focalised by the MM on a thinned backside illuminated CCD through different filters. The available filters are :

- a 8 mm meshless Al filter for measurements at 58.4 nm,
- a 40 mm Al meshed filter covering all the CCD for extrafocal imaging at 58.4 nm,
- a 8 mm Al-C for measurements at 30.4 nm,
- an open position, a 620 and 410 nm interferential filter are available for visible measurements,
- a shutter.

A schematic view of the EUV channel is shown in figure 1. All the optical parts are on a rigid optical bench, mechanically decoupled from the ground vibrations. Four photomultipliers are installed in the parallel beam to check the stability and the homogeneity of the output beam. A conjugate laser source is available for alignment purposes. From a command room, two workstations manage the facility, one mainly for temperature and pressure control and displacement, and a second one for image acquisition and data handling. At the end of each test the images are recorded on CD-ROM. Analyses are carried out on site, using homemade software. This allows getting real time diagnostics, to take fast decisions and to modify the test procedures if required.

3.3. PSF measurements at 58.4 nm

The MM is aligned under vacuum with respect to the EUV collimated beam by maximising the throughput vs. the Field Of View (FOV). Once the MM is correctly aligned, a best focus search is performed by stepping along the X-axis with steps of 2 mm and computing HEW at each step. The designed focal length is 7500 mm from the parabola – hyperbola interface for all the MMs, the measured one is about 6 mm shorter. Less than 1 mm difference in focal length is measured between all the FM MMs. The PSF best focus images of the five MMs are presented in figure 2. From the first model to the last one, an improvement of the PSF shape, is observed and is reflected in the values of Half Energy Width (HEW) and Full Width at Half Maximum (FWHM) as summarised in Table 3. In terms of HEW a significative improvement was reached between QM and FM1 (19 to 15.5 arcsec). No improvement is noticed between FM1 and FM2, mainly due to an imperfect integration of the Mirror Interface Structure[8] (MIS). The MIS is the cylinder surrounding the 58 MS interfaced with the spider. Stresses between the MS and the spider are dramatic for the image quality. For all the FM MMs the core of the PSF presents a very sharp and unique peak (this was not the case with the QM). The HEW is better than the requirements (16.5 arcsec), and the 90EW is decreasing due to the improvement of the mirror shell edges geometry. FM3 and FM4 present a fairly good shape. The achieved HEW for these two last FM MMs is close to 14 arcsec!

Table 3 : HEW, 90EW and FWHM computed at best focus for QM and for FM MMs

Mirror Module [arcsec]	QM	FM1	FM2	FM3	FM4
HEW	19	15.5	15.4	14.1	14
90EW	79	62.6	62.5	59.2	60.7
FWHM	11	6.7	6.3	4.5	4.9

Figure 2: 2D view in log scale of the best focus PSF

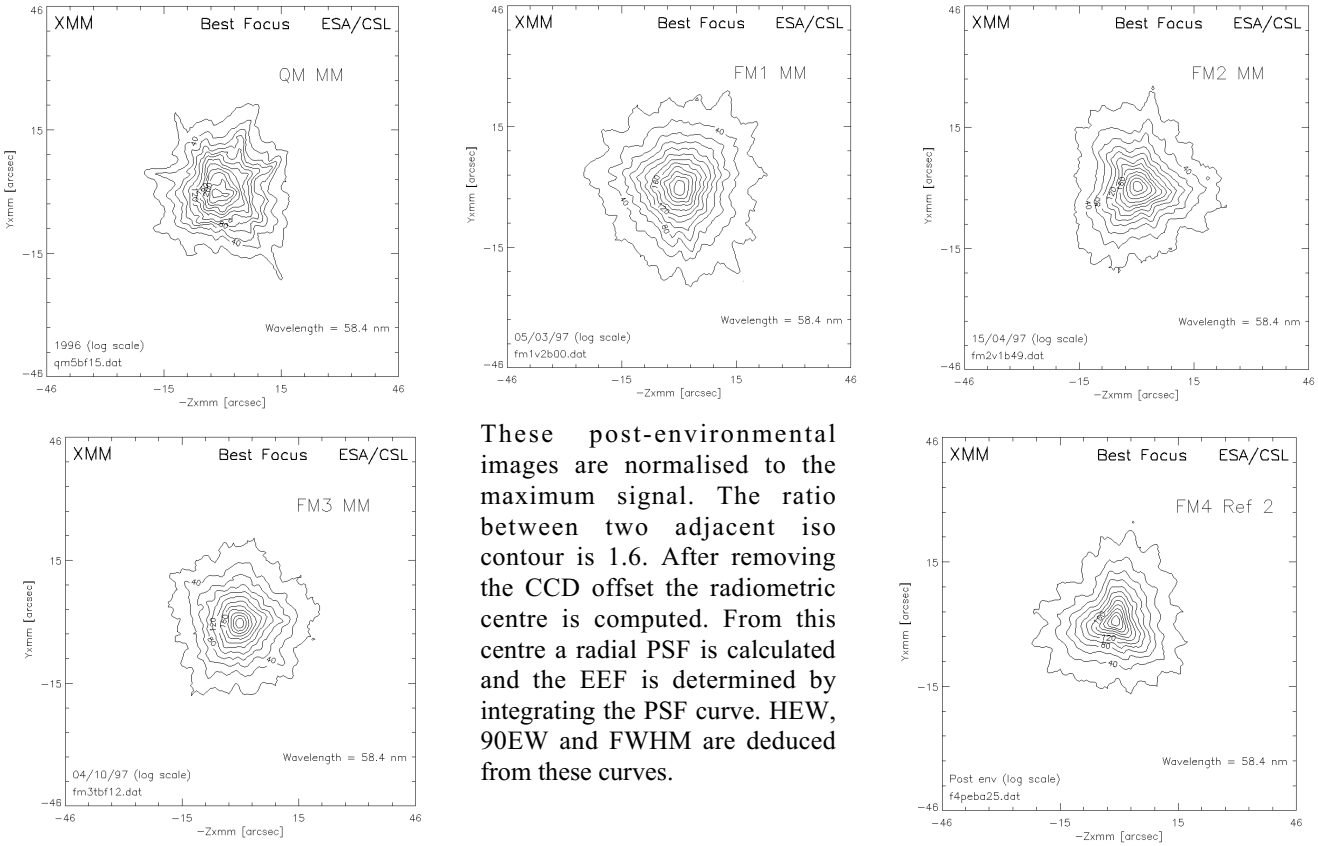

These post-environmental images are normalised to the maximum signal. The ratio between two adjacent iso contour is 1.6. After removing the CCD offset the radiometric centre is computed. From this centre a radial PSF is calculated and the EEF is determined by integrating the PSF curve. HEW, 90EW and FWHM are deduced from these curves.

4. XRB INTEGRATION AND EFFECTIVE AREA ON-AXIS AND OFF-AXIS

Straylight analysis has shown[4] that an X-Ray Baffle (XRB) must to be integrated on each MM, to reduce the straylight coming from objects close but outside the MM FOV (+/- 15 arcmin). The XRB consists of 2 sieve plates, axially spaced by 54 mm and put at 85 mm in front of the MM entrance plane[4]. This baffle is equivalent to extend the mirror shell forward. It "precollimates" the incoming beams and by this way reduces single reflection hyperbola path. Particular care is taken in the XRB design to reduce the scattering, the diffraction and undesired reflection induced by the baffle itself. The XRBs have already been integrated on FM1 and FM2 MMs. Tests are performed to demonstrate that the optical performance in terms of HEW and effective area are not degraded.

For what concerns the HEW, 90EW and FWHM, the observed variations are inside the measurement accuracy. No degradation of the on axis effective area is observed before and after XRB integration. The relative off axis effective area is plotted in figure 3. The reduction of effective area in the FOV presents a symmetric behaviour, which shows a correct integration. A good correlation of the measurements with the theoretical model is observed and gives confidence in the quality of the XRB integration and manufacturing.

Figure 3 (right) : Relative effective area in the FOV for 2 orthogonal azimuths (rotation around Y_{XMM} labelled Az=0° and Z_{XMM} labelled Az = 90°). The lines represent the simulated data, the points the experimental data. (-XRB means without XRB and + XRB means with XRB).

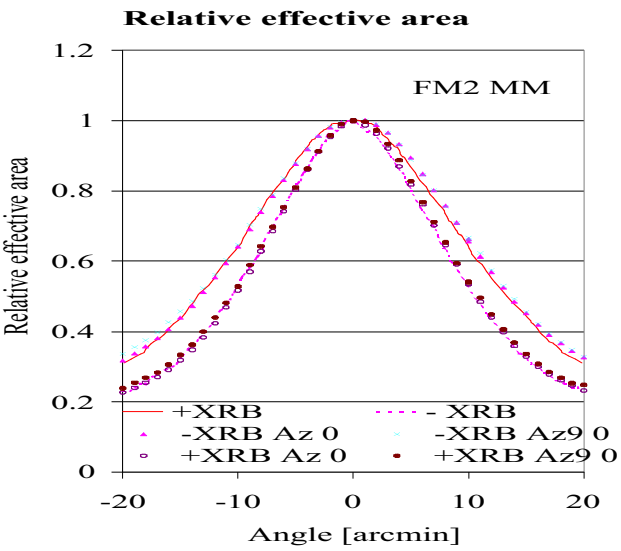

5. STRAYLIGHT TESTS

The goals of the straylight tests are to verify the XRB efficiency in terms of straylight reduction. This is performed by recording images for objects between 20 arcmin and 7 arcdeg off axis, in the visible and in the EUV. To reach these angles, the whole optical bench is tilted with respect to the collimated beam axis (see figure 4). With this procedure, the MM and the EUV CCD detector move together as an individual telescope. The EUV CCD has an 18 * 25 mm_ sensitive area. To cover the 66 * 66 mm_ of the XMM detector, the EUV CCD is translated at 9 locations. A mosaic is realised to reconstruct the straylight image as presented in the figures 6. Figures 6.a and b show the straylight distribution in the XMM detector field of view for an EUV source point positioned at 30 arcmin. The figure 6.a is the distribution before XRB integration. The observed rings correspond to single hyperbola reflection. When the XRB is integrated (figure 6.b), the rings are clearly attenuated. The reduction of straylight is confirmed by computing the effective area over each of these mosaic images (figure 5).

Figure 4 : Tilt of the optical bench for straylight measurement

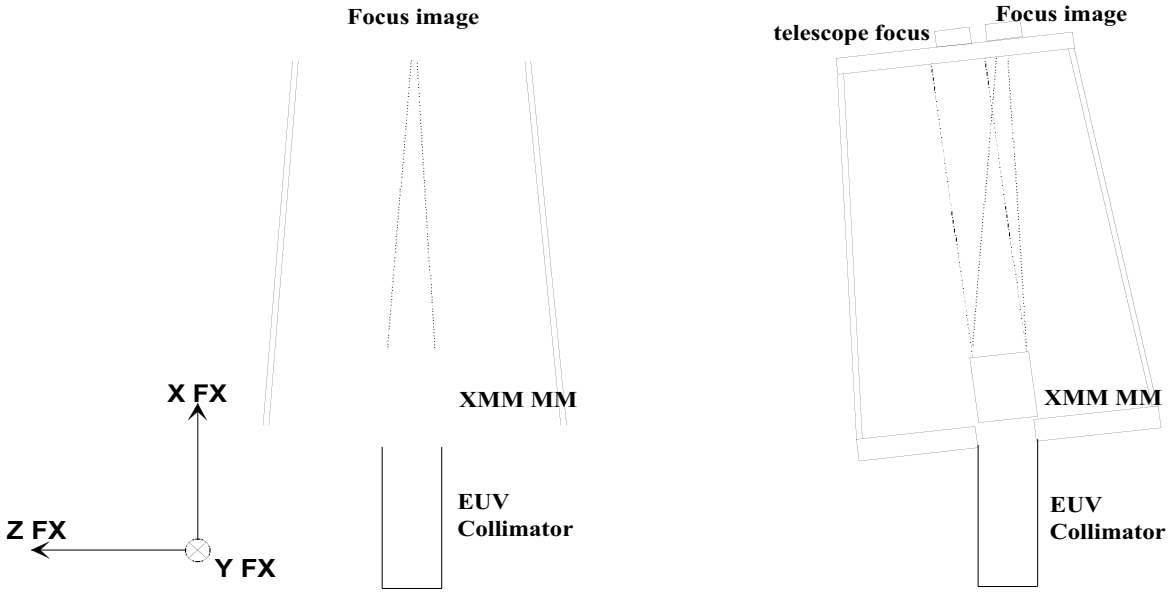

The theoretical data comes from[14] an analysis performed by BRO with the ASAP software. This model shows good correlation with the experimental data. An attenuation of a factor 5 by the XRB is noticed as expected. The observed difference between theory and experiment at 30 arcmin comes from the presence of the ghost image (see figures 6). Its effect in terms of effective area corresponds to a few cm_ in the EUV. Stray lines have been drawn between the available data (experimental and simulated ones).

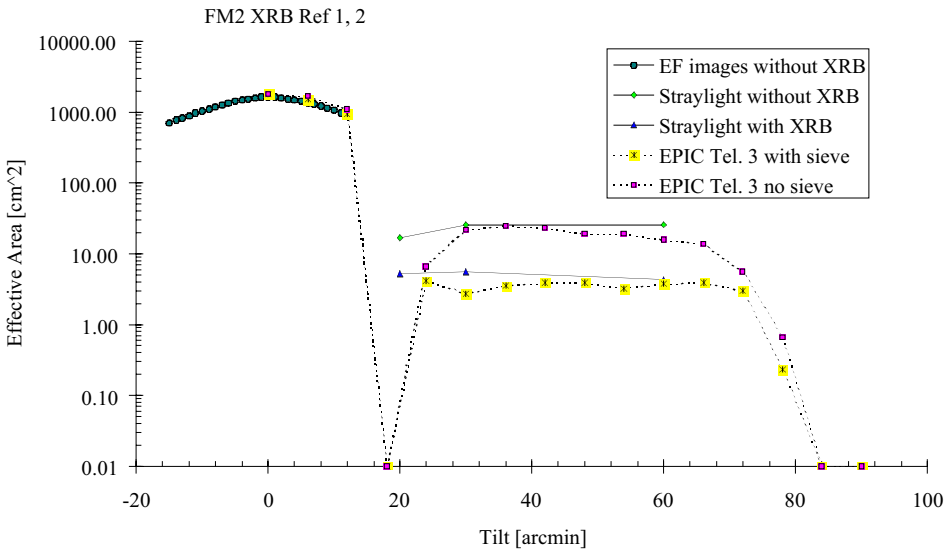

Figure 5 : Effective area in the telescope detector area vs. FOV at 58.4 nm.

For FM1 and FM2 MMs, an unexpected "ghost image" appears between 20 and 40 arcmin (see figure 6.a). This one is not observed in the simulation (Figure 7.a.). On FM3 and FM4 MMs the "ghost image" is strongly attenuated. Quantitative analyses are only available on FM2 MM. They show a straylight reduction on FM2 MM, but not as efficient as expected due to the presence of the "ghost image" (see figure 5). The XRB has no impact on this "ghost image". The origin of this "ghost image" is not yet clearly understood. Simulation shows that the "ghost image" doesn't come from Ni back side reflections of the MSs. The simulation doesn't take into account the MS distortion. The "ghost image" doesn't come from the facility itself, since several mechanical configurations have been tested and the "ghost image" is weaker on FM3 and FM4 MMs. The optical path of the ghost arises from 2 sectors of the MSs 25 to 35 depending on the MM orientation. A sketch presenting the ghost image origin from the output of the MM is presented in figure 7.b.

Figure 6.a (left) and b (right) : Straylight distribution from a point source located at 30 arcmin in the equivalent XMM detector sensitive area. These figures are a mosaic reconstruction of 9 CCD images. The centre of the image is the centre of EPIC area. Some parts of the images are missing due to vignetting. The figure on the left is recorded before XRB integration. The right one with XRB integrated. The acquisition parameters and the data handling are the same for both images. The attenuation of the hyperbola single reflection is obvious (bottom rings on both images).

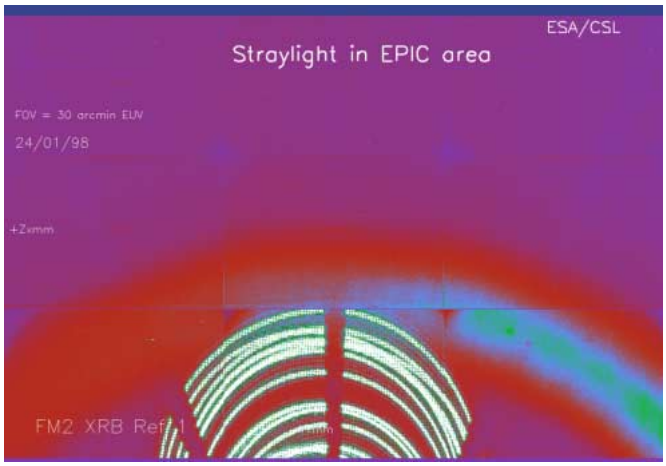

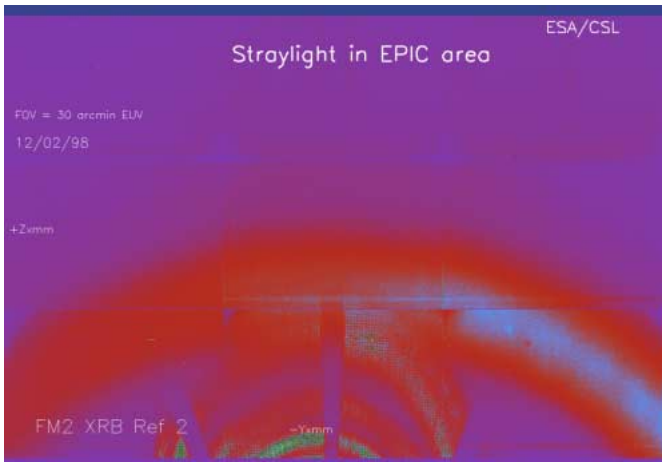

Figure 7.a. : Simulated image at 30 arcmin in EPIC area (scale and position are not exactly respected between simulation and measured picture (figures 6)). The last rings on the measured picture correspond to mid MSs that are deformed. This deformation is not introduced in the simulation.

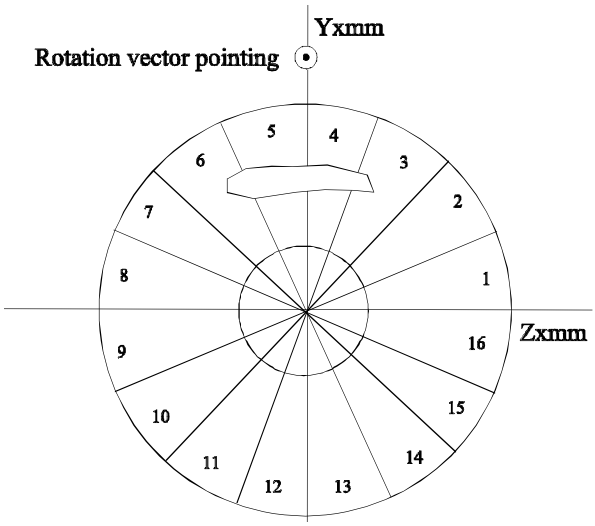

Figure 7.b. : Origin of the ghost image

Figure 7.b. presents the origin of the straylight from the MM exit plane viewed from the detector. This one is localised between MSs 25 to 35 and in sector 5 to 4 when the rotation is performed around Zxmm clockwise. This situation corresponds to the images of figures 6.

In conclusion, the X ray baffle has the expected efficiency. The presence of a "ghost image" is not yet completely understood. Simulations taking into account facility straylight and / or MM defaults are still running. The ghost image is MM dependent, but is in any case very weak (a few cm_).

6. X-RAY REFLECTIVITY MEASUREMENTS

6.1. Introduction

One of the most important requirements for XMM on-ground calibration is the determination of the effective area. This is required because of the absence of "standard cosmic" X-ray sources, that could be used for in-orbit calibration. Several methods have already been used[6,10]. The partial illumination methods is a good approach to compute the effective area in the X-ray range. These methods provide the effective area taking into account the loss by reflectivity and the loss by vignetting. These are the main contribution to the effective area value. The method applied at CSL assumes that the local reflectivity on one point of the MS is representative of all the MS. This method doesn't take into account the geometry. After a brief presentation of the test configuration, the paragraph will mainly deal with the results achieved on FM1 and FM2 MMs.

6.2. X-ray pencil beam set-up

Figure 8 illustrates a general layout of the pencil beam set-up[6,7]. At the bottom end of this channel, an X-ray source equipped with 5 different anodes (Al, Au, C, Cu, Mo) provides several spectral lines from 0.2 to 13 keV. A filter wheel put in front of the source allows to select the lines and to remove the visible part of the source emission. The collimator consists in 2 pinholes of 0.3 mm diameter separated by 7540 mm. This provides a slightly divergent pencil beam of 0.5 mm diameter at MS level.

The beam is bent to the telescope focal plane by the parabola and hyperbola combination. In the focal plane, two detectors are available, one front side CCD detector for imaging purpose and one Germanium solid state detector of 20 mm diameter for spectral purposes. The solid state detector is closed with a mesh supported Be window transmitting 55 % at 1.5 keV and 85 % at 8 keV. The cooling of the detector is performed via a small liquid nitrogen reservoir connected to the detector cold finger by copper straps. A second solid state detector is located just in front of the second pinhole to monitor the incident flux during the reflectivity measurements. The CCD is a front side illuminated detector working in frame transfer and in photon counting mode.

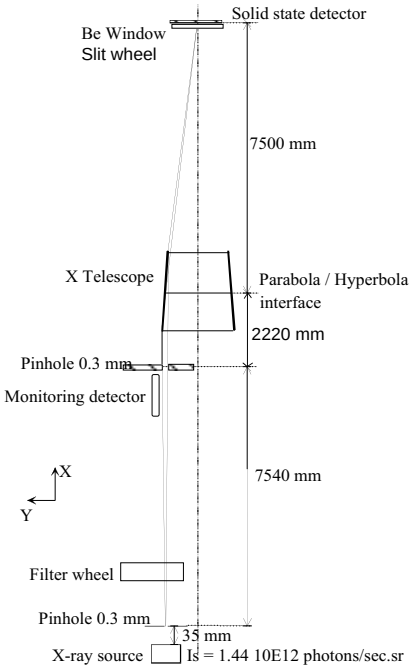

Figure 8 : X-ray pencil beam channel General layout

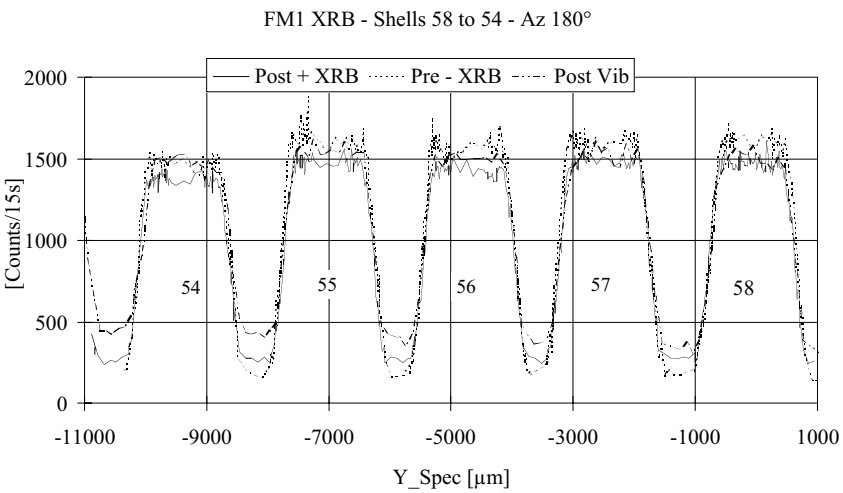

Figure 9 : Detail of a scan on FM1 MM MS 58 to 54. These scans are performed at 1.5 keV. 3 scans have been performed on FM1. A first used as reference, a second after XRB integration and a third after vibration test. To save time a sample of MSs is scanned : 5 small MSs and 5 large MSs. This is performed around 4 orthogonal azimuths. The plot shows that there is no on axis vignetting due to the presence of the XRB.

6.3. X-ray reflectivity measurement

The following procedure is used to measure the reflectivity. First, the MS positions are determined by scanning the MM in front of the pencil beam[8]. During these scans the Solid State Detector (SSD) moves synchronously with the MM. The data are also used to verify the good positioning of the XRB and to check the stability during the environmental tests. An overplot of such scans before and after environmental tests is presented in figure 9. Once these scans are performed the MS and the SSD positions are determined so that the middle position of each mirror shell parabola is known for reflectivity measurements.

The reflectivity is measured by recording the reflected flux of each MS and the direct flux every five reflected flux measurements. During the measurement the flux stability is monitored by a diode, and checked by the X-ray source voltage and current between each measurement. The reflectivity value of the MS is simply the ratio of the counts in the region of interest of the reflected and incident fluxes. These measurements have been performed at the following energies:
1.5, 2.1, 2.29, 8, 8.9, 9.7 and 11.5 keV.

6.4. Results and analysis

The grazing angle varies on each MS, so that a graph of the reflectivities vs. the grazing angle can be plotted as presented in figures 10. These plots are then compared to the theoretical curves. The theoretical curves use the Fresnel equation with n and k taken from "Palik"[15] refraction index table. The fit is not perfect. Several corrections must be done on the raw data. The first one is to take into account the loss by scattering in the reflected flux due to the limited size of the SSD. Wing scattering measurements at 1.5 and 8 keV show that the loss at 1.5 keV is 0.6 % and at 8 keV is 6%, that means an energy square dependence. This correction is applied at all the energies. The next correction performed is to tilt the MM until the best fit is achieved. This exercise was only needed on FM1 MM, where a tilt of 30 arcsec was required.

To evaluated the effective area of a MM, from these reflectivity data, the following formula is applied :

$$Eff\_area = \sum_{i=1}^{58} R_i * Geom\_area_i$$

where R_i is the measured reflectivity and $Geom\_area_i$ is the designed geometrical area of the i^{th} MS.

Figure 10 : Reflectivity data of FM1 MM at 9.7 keV and FM2 MM at 8 keV

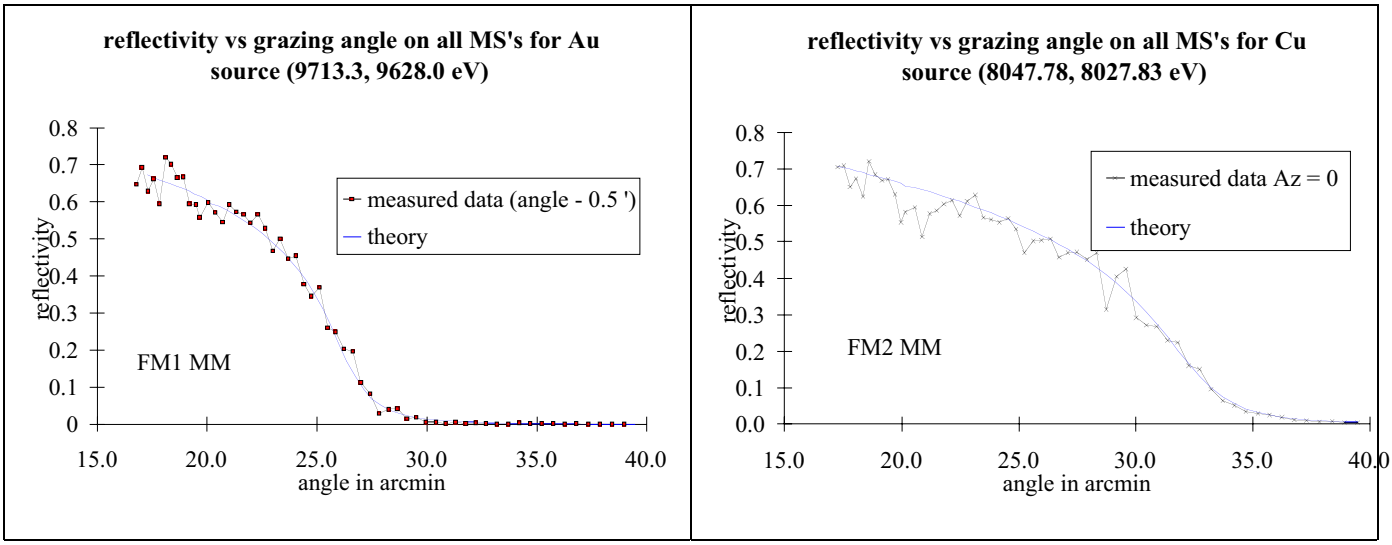

The result of this computation over the available energies is presented in the figure 11 for FM1 and FM2 MM. The results are close to each other (differences about 1 % for energies lower than 8.9 keV). These results are compared to the effective area measured at MPE Panter facility[10]. The MPE data at 0.28, 1.5 and 8 keV for FM2 MM are available. The observed differences with the present method is less than 1% at 1.5keV and 4 % at 8 keV. These results are compared to the theoretical value as it is done on the plot of figure 11. The worst correlation at higher energy (8 keV) is not yet clearly understood. Two ways are investigated : a) introduction in the scattering correction of the incident angle, b) the measurements at these energies are very sensitive to the MS slope error (incident angle variation). The method has shown reproducibility in effective area of 1% during FM4 MM tests. A correlation is observed between the loss of reflectivity and the surface microroughness quality. The poor surface microroughness quality provides a high amount of scattering, this underevaluates the reflected flux.

Figure 11 : Effective area results for FM1 and FM2 with pencil beam reflectivity data

	theory	*measured*	*measured*	*Diff*	*FM2*
energy	*effective*	*Taking*	*taking*	*In %*	*MPE*
keV	*area*	*scattering*	*scattering*	***FM1/***	Value
	[cm_]	**FM1**	**FM2**	***FM2***	*Cm_*
	spider out				*Dif %*
1.50	1486	1429.6	1407.6	**1.54**	**1421.7**
2.10	1293.7	1283.5	1270.3	**1.03**	**-0.55**
2.29	917.9	892.8	894.4	**-0.18**	
8.00	622.2	593.8	599.8	**-1.01**	**618.3**
8.90	461.	477.9	480.8	**-0.60**	**4.13**
9.70	346.00	374.5	363.1	**3.05**	
11.50	157.7	174.4	167.0	**4.23**	

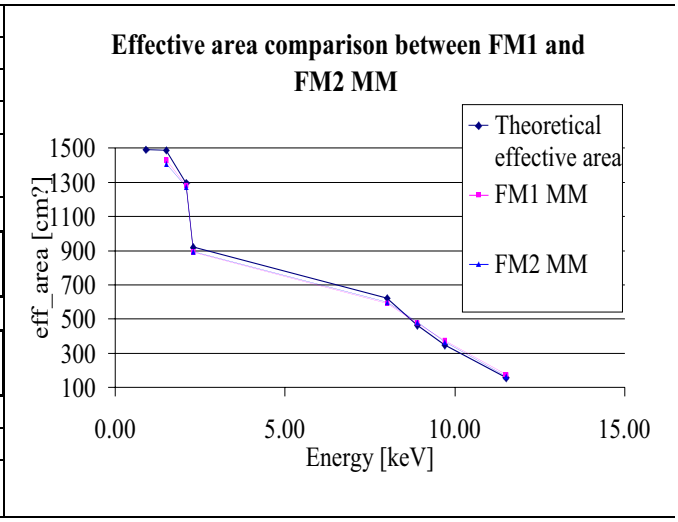

7. WING SCATTERING DATA

7.1. Introduction

Once the MSs are integrated in the MM, there is no way to measure directly their microroughness. The way used at CSL to verify that there is no degradation of the MS surface microroughness quality between the environmental tests is to measure the angle resolved scatter. Modelisation of the angle resolved scatter with the PROMAP data is performed. This allows to calibrate the scattering effect in the XMM numerical model[11].

First the procedure to acquire the data is presented. Then the way the correlation is achieved with the microroughness measurement before integration is explained.

7.2. Wing scattering measurement

The X-ray pencil beam channel is used as for the reflectivity measurement. A small X-ray pencil beam illuminates about 100 mm of a MS parabola. The position of the MS is the one used for reflectivity measurement i.e. the centre of the MS parabola. The beam is reflected to a front side CCD detector working in frame transfer mode. The active area is 800 x 576 pixels of 22.5 x 22.5 µm_.

Before starting the acquisition, the CCD is set up to work in photon counting mode, and the spectral quality of the beam is checked. Then 1000 frames are recorded, and only the pixels with a signal higher than a calibrated threshold are transferred to the data file. Once the recording is finished, the columns of the image file are added. The results is a wing scattering profile, with a resolution of 22.5 µm. At high energies, the X-CCD detector is translated twice by 15 mm on each side of the central spot image, in order to record the scattered wings. Small overlapping between the image allows to connect properly the data. The whole image gives a profile over 45 mm, i.e. slightly more than 1200 arcsec (see figure 12).

7.3. Data analysis

The simplest way to check the impact of the environmental test is to overplot the wing scattering data from the various reference tests (figure 12.a). This only confirms that there is no degradation of the gold layer due to the environmental tests. A more fruitful exercise is to check the matching of the microroughness data to the angle resolved scatter. This is performed by using the Rayleigh Rice theory[12,13], taking into account the reflection on the parabola and hyperbola surfaces. The core of the angle resolved scatter is modelled by a Gaussian, the wings are fitted with the average power spectral density measured on the same MS with the PROMAP microscope interferometer. In conclusion the method shows that there is no impact of the environmental tests on the optical surface, but also a good correlation between measurement performed before integration of the MS in the MM, this means no impact of the integration on this parameter. This confirms that the PROMAP data can be used on all the MS in the XMM numerical model[11].

Figure 12.a : Comparison before and after environmental tests. The good superposition of the curves demonstrates no degradation of the surface microroughness.

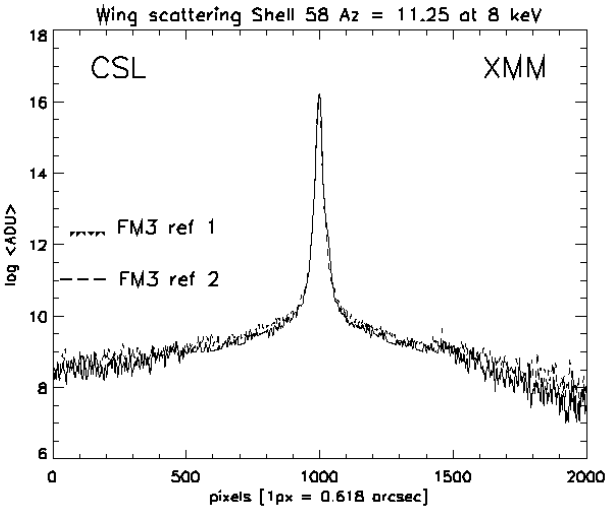

Figure 12.b : Comparison between experimental results and best fit angle resolved scatter with the average PSD measured.(the smoothed curve is the fitted one)

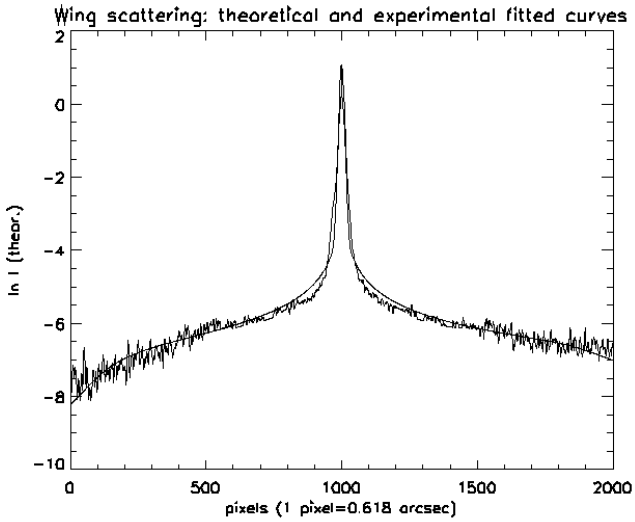

8. CONCLUSIONS

XMM satellite is foreseen to be launched in August 1999. Four Flight Model Mirror Modules have been manufactured and tested, and all of them are better than the specifications in terms of image quality. The set of optical tests performed at CSL shows that thermal constraints and launch conditions don't deteriorate the optical performance of the MMs. A simple way to measure effective area has been presented and shows very good correlation with respect to accurate measurement method. They confirm that the FM1 and FM2 MMs effective areas are inside the required specification. The control of the integration and the efficiency of the X-ray baffle has also been performed during straylight tests. Interesting observation were performed, showing unexpected straylight on FM1 and FM2 MMs, but 3 times weaker on FM3 and FM4 MMs. These tests show that the integration of the MS is an activity that has to be performed with great care. Any small change in the procedure introduces a different stress between MS and the spider. This can completely modify the telescope behaviour.
Before the end of 1998, XRB has to be integrated on FM3 and FM4 MM and will be tested at CSL (optically and environmentally) before the delivery to the prime contractor. At the end of all these tests 3 MMs will be selected out of the 4 to be integrated on the satellite.

Acknowledgements

Our first thanks go to our colleagues who worked hard for already 3 years on the XMM MM testing. Their work is greatly appreciated and is a key factor in the collection and quality of the data.
Many thanks go to ESA XMM project team for the fruitful relations and collaborations.
The vertical facility at CSL was funded by ESA XMM project under the contract number 9939/92/NL/PP.
The XMM FM MM mirrors were replicated and integrated by MEDIA LARIO under ESA contract number 0545/93/NL/RE.

References

1. D. de Chambure, R. Lainé, K. van Katwijk, J. van Casteren & P. Glaude, "Producing the X-Ray Mirrors for ESA's XMM Spacecraft", ESA bulletin 89, February 1997.
2. R. Lainé, D. de Chambure, D. Kampf, G. Grisoni, "Results of thin X-ray mirror technology for ESA XMM Mission", 48th IAF Congress, Torino, Italy, 1997.
3. F. Jansen, "XMM Observatory : a scientific and technical overview", These Proceedings
4. D. de Chambure, K.van Katwijk, R. Lainé, J. van Casteren, G. Peterson, M. Côté, B. Aschenbach, R. Willingale, D. Schink, A. Frey, W. Rühe, Y. Gutierrez, F. Draheim, "Reducing the optical and X-ray stray light in the ESA XMM telescope", ICSO, Toulouse (France), 1997.
5. Y. Stockman, I. Domken, H. Hansen, J.Ph. Tock, T.A. Decker, A. Rasmussen, T. den Boggende, J.W. den Herder, G. Bagnasco, D. de Chambure, C. Erd, Ph. Gondoinl, "XMM Flight Mirror Module with Reflection Grating Assembly and X-ray baffle testing", SPIE 3445 , San Diego 1998.
6. J. Ph. Tock, J-P. Collette, Y. Stockman, "Calibration and upgrades of the XMM vertical EUV/X test facility; FOCALX", SPIE 3114, pg 554, San Diego 1997.
7. J Ph Tock, J P Collette, I Domken, Ph Kletzkine, Y Stockman, A Vignelles, " FOCAL X : A test facility for X-ray telescopes", 3rd International Symposium on Environmental Testing For Space Programmes, Noordwijk 1997
8. Y. Stockman, J-P. Collette, J. Ph. Tock, "Optical testing of XMM flight model module I and II at the vertical EUV/X facility", SPIE 3114, pg 566, San Diego 1997.
9. O. Citterio, P. Conconi, M. Ghigo, C. Jamar, R. Loi, F. Mazzoleni, G. Naletto, E. Pace, Y. Stockman, G. Tondello, P. Villoresi, "Vertical test facility operating at vacuum ultraviolet for testing very thin wall grazing incidence X-ray mirrors", SPIE Vol. 2279, 1994.
10. R. Egger, B. Aschenbach, H. Brauninger, W. Burkert, T. Döhring, A. Oppitz, "X-ray calibration of the XMM flight mirror at the Panter test facility", These proceedings.
11. P. Gondoin, "Calibration status of the XMM FM Mirror Module", ESTEC/Astrophysics, Status report 02/17/98
12. J. C. Stover, "Optical scattering measurement and analysis", Mc Graw-Hill, 1990.
13. Ph. Gondoin, B. Aschenbach, M. Deijersbergen, R. Egger, F. Jansen, Y. Stockman, J.P.Tock, "Calibration of the first XMM Flight Mirror Module I – Image Quality", These proceedings.
14. G. L. Peterson, M. Coté, "Straylight analysis of the XMM telescope", BRO report #3000, Final report 09/30/96.
15. E. Palik, "Handbook of Optical Constants of Solids", Academic press, 1985.